Published in final edited form as:
Coord Chem Rev. 2013 January 1; 257(1): 110–118. doi:10.1016/j.ccr.2012.05.038.

Applications of pulsed EPR spectroscopy to structural studies of sulfite oxidizing enzymes☆

Eric L. Klein, **Andrei V. Astashkin**, **Arnold M. Raitsimring**, and **John H. Enemark***
Department of Chemistry and Biochemistry, University of Arizona, Tucson, AZ 85721-0041, USA

Abstract

Sulfite oxidizing enzymes (SOEs), including sulfite oxidase (SO) and bacterial sulfite dehydrogenase (SDH), catalyze the oxidation of sulfite (SO_3^{2-}) to sulfate (SO_4^{2-}). The active sites of SO and SDH are nearly identical, each having a 5-coordinate, pseudo-square-pyramidal Mo with an axial oxo ligand and three equatorial sulfur donor atoms. One sulfur is from a conserved Cys residue and two are from a pyranopterindithiolene (molybdopterin, MPT) cofactor. The identity of the remaining equatorial ligand, which is solvent-exposed, varies during the catalytic cycle. Numerous *in vitro* studies, particularly those involving electron paramagnetic resonance (EPR) spectroscopy of the Mo(V) states of SOEs, have shown that the identity and orientation of this exchangeable equatorial ligand depends on the buffer pH, the presence and concentration of certain anions in the buffer, as well as specific point mutations in the protein. Until very recently, however, EPR has not been a practical technique for directly probing specific structures in which the solvent-exposed, exchangeable ligand is an O, OH^-, H_2O, SO_3^{2-}, or SO_4^{2-} group, because the primary O and S isotopes (^{16}O and ^{32}S) are magnetically silent ($I = 0$). This review focuses on the recent advances in the use of isotopic labeling, variable-frequency high resolution pulsed EPR spectroscopy, synthetic model compounds, and DFT calculations to elucidate the roles of various anions, point mutations, and steric factors in the formation, stabilization, and transformation of SOE active site structures.

Keywords

Sulfite oxidase; Molybdenum enzymes; Electron paramagnetic resonance (EPR); Electron spin echo envelope modulation (ESEEM); Isotopic labeling; Density functional theory (DFT)

1. Introduction

Sulfite oxidizing enzymes, including sulfite oxidase (SO) and sulfite dehydrogenase (SDH), catalyze the physiologically essential two-electron oxidation of sulfite to sulfate (Eq. (1)) [1,2]. In plants and vertebrates, SO functions in the final metabolic degradation step of sulfur-containing compounds and serves to eliminate toxic sulfite from the organism [3]. The electrons from this process are ultimately passed on to either ferricytochrome *c* (cyt *c*) in vertebrates or to molecular oxygen in plants [4]. In contrast, certain bacteria use SDH to catalyze the oxidation of sulfite from thiosulfate, which they use as an energy source [5].

☆In celebration of the 65th birthday of Prof. Edward I. Solomon.

*Corresponding author. Tel.: +1 520 621 2245; fax: +1 520 626 8065. jenemark@email.arizona.edu (J.H. Enemark).

$$SO_3^{2-} + H_2O \rightarrow SO_4^{2-} + 2H^+ + 2e^- \quad (1)$$

Although the tertiary structures of the SO [6,7] and SDH [8] proteins differ considerably from each other (Fig. 1), the active site structures of these enzymes, at least with respect to their catalytic Mo centers, are practically identical (Fig. 2a). In each case, Mo is coordinated by a total of five ligand donor atoms in the same pseudo-square pyramidal geometric arrangement: an axial oxo group (O_{ax}), an equatorial sulfur from a conserved Cys residue, two sulfurs from a pyranopterindithiolene cofactor (molybdopterin, MPT), and an exchangeable equatorial ligand whose identity depends on the stage of the catalytic cycle, specific protein point mutations, and the buffer conditions in which the enzyme is prepared (Fig. 2b). In the fully oxidized Mo(VI) resting state of SOEs, this equatorial ligand is also an oxo group (O_{eq}) [9]. For the pathological R160Q mutant of human SO (hSO), it has been suggested that a nearby Gln residue (substituting the conserved non-coordinating Arg residue that is located immediately *trans* to O_{ax} in the *wt* enzyme) also coordinates to form a 6-coordinate Mo center [10]. However, recent results obtained using pulsed electron paramagnetic resonance (EPR) techniques in conjunction with isotopic labeling and density functional theory (DFT) argue that the Mo center of this mutant remains five-coordinate in a pseudo-square-pyramidal geometry (*vide infra*) [11].

The boxes of Scheme 1 show a simplified catalytic cycle for the oxidation of sulfite by SOEs [1]. The initial reaction of sulfite with the dioxo-Mo center (**1**) reduces the fully oxidized Mo(VI) (d^0) state to Mo(IV) (d^2), forming the enzyme-product (EP) complex (**2**). Mo(IV) is reoxidized to the Mo(VI) resting state by two sequential one-electron oxidations, passing through the paramagnetic Mo(V) (d^1) intermediate (**3**). In the vertebrate and bacterial enzymes these sequential one-electron oxidations involve intramolecular electron transfer (IET) to their integral heme centers [3].

The exact order of IET and product release in going from **2** → **3** in Scheme 1 is still a matter of debate. A mechanism in which hydrolysis of the product, sulfate, occurs prior to any Mo(IV) oxidation step has been most frequently invoked [1]. However, pulsed EPR studies of the paramagnetic Mo(V) state of plant SO at low pH suggested that electron transfer from Mo(IV) could precede hydrolysis [12,13], as indicated by **2** → **4** in Scheme 1. The formation of this so-called “blocked” Mo(V) form (**4**) is also consistent with the fact that the enzyme turnover rates of SOEs are known to be much slower than their IET rates [3,14,15]. Because of the large excess of substrate (sulfite) present in the EPR studies, structure **5** with bound sulfite is another possible species that may be formed. Indeed, a sulfite-containing Mo(V) species was originally proposed in the early 1980s by Bray et al. [16]. Evidence for **4** and **5** is discussed in Section 3.

Historically, EPR has been an extremely important technique for probing the Mo(V) states of SOEs and for obtaining information about specific Mo(V) structures [16–19]. However, it can be difficult to distinguish among structures in which the solvent-exposed, exchangeable ligand is a O^{2-}, OH^-, H_2O, SO_3^{2-}, SO_4^{2-}, or PO_4^{3-} group since the primary O and S isotopes (^{16}O and ^{32}S) are magnetically silent ($I = 0$). Only those ligands that also contain magnetic nuclei (*e.g.*, protons (^1H, $I = 1/2$), deuterons (^2H, $I = 1$), or phosphorus (^{31}P, $I = 1/2$)) can provide the hyperfine interactions (*hfi*) or nuclear quadrupole interactions (*nqi*) needed for structure determination. Consequently, most of the early EPR spectroscopy of SOEs was centered on broad comparisons of the electronic *g*-values between different states of the enzymes prepared under a variety of conditions. Such studies provided the first valuable information about the specific structural or chemical differences at the Mo(V) centers that produced the various spectroscopic results (Fig. 3). For example, the CW EPR spectra of vertebrate SO prepared at relatively low pH values (pH ~ 6) show a strong

hyperfine coupling with a single exchangeable proton, indicative of an OH ligand. In contrast, at relatively high pH values (pH ~ 9), the CW EPR spectra show no observable proton *hfi*, and somewhat different *g*-values are observed [17]. However, high-resolution pulsed EPR experiments at high pH indicate significant *anisotropic hfi* with the exchangeable proton from the OH ligand [20,21]. In the high-pH (*hpH*) form of the enzyme, it is now known that the OH ligand adopts orientations that allow only minimal overlap of the O H bond with the Mo(V) d_{xy} orbital, which has the principal unpaired electron character. Thus, the *isotropic hfi* of the OH proton at high pH is extremely small, yet the anisotropic *hfi* is significant. For the "phosphate inhibited" (P_i) form, coupling to 31P (I = 1/2) was postulated from the third-derivative CW EPR spectra [22]. Subsequent pulsed EPR experiments provided definitive evidence for a coordinated phosphate in the place of the OH group [23,24]. More recently, the introduction of ^{33}S and ^{17}O labels (I = 3/2 and 5/2, respectively) has allowed additional exchangeable ligands of the Mo center to be directly probed [13,24,25]. More detailed structural determination from EPR measurements, however, relies on the comparison of the experimental spectroscopic parameters with those of analogous structurally defined model complexes and/or DFT computational models of the enzyme active sites.

Based on the CW EPR results obtained for vertebrate SO in the 1980s, three general forms of the enzyme (SOEs) were identified: "high pH" (*hpH*); "low pH" (*lpH*); and "phosphate-inhibited" (P_i) [17]. Since then, complexes with other oxyanions, including arsenate [26] and sulfite [24], have also been prepared and identified. This review summarizes some recent advances in the use of isotopic labeling, variable-frequency high resolution pulsed EPR spectroscopy, synthetic model compounds, and DFT calculations to elucidate the roles of various anions, point mutations, and steric factors in the formation, stabilization, and transformation of SOE active site structures in each of these unique forms.

2. The high-pH form

Early CW EPR experiments on *wt* SOEs revealed that the spectra of the enzymes prepared in high pH buffers (pH ≥ 9) differ considerably from those obtained at neutral or slightly acidic pH values (Fig. 3). In addition to each of the principal *g*-values (g_x, g_y, and g_z) of the spectra being smaller than the respective values at low pH, there are no resolved proton couplings at any of the *hpH* form EPR turning points. This observation was initially interpreted to simply reflect the deprotonation of the equatorial OH group at high pH. George, however, proposed that Mo OH could also be present at high pH, despite the lack of observable *hfi* [27]. Furthermore, some experimental support for the existence of the OH ligand in the *hpH* form had already been reported in a ^{17}O (I = 5/2) study by Cramer et al., in which the ^{17}O *hfi* was observed in the X-band CW EPR spectra for both the *hpH* and *lpH* forms and was assigned in both cases to a water-exchangeable oxygen-containing ligand, most likely OH, coordinated to Mo(V) [28]. Pulsed EPR experiments reveal two other unique ^{17}O species, each of which has a much smaller *hfi* than the OH ligand [29]. These have been assigned to the axial oxo (O_{ax}) and to an outer-sphere OH (or possibly sulfite/sulfate) that is hydrogen-bonded to the OH ligand. The very different exchange rates for the equatorial and axial oxo ligands provide a convenient method of "isolating" the contribution of the equatorial ligand when the enzymes are only briefly exposed to the ^{17}O-enriched buffer before being reduced with sulfite [29].

As mentioned above, the observation of ^{17}O *hfi* in the CW EPR spectra of *hpH* SO was the first indication of a possible OH ligand in the *hpH* form of SOEs. The assignment of the ^{17}O signal to OH rather than to some other oxygen-containing ligand that could exchange with ^{17}O-enriched buffer, however, could not be confirmed without detecting the OH proton

directly. The detection of this proton was eventually accomplished through a series of pulsed EPR experiments [20,21].

Pulsed EPR spectroscopy has substantially higher resolution than CW EPR, and the K_a-band (~30 GHz) ESEEM experiments allowed the variation of the ^{17}O *hfi* to be followed as a function of the EPR position, so that the isotropic and anisotropic parts of the *hfi* could be evaluated separately. The results of these ^{17}O *hfi* measurements for several enzymes are presented in Fig. 4. We note that the *hfi* constants shown in Fig. 4 are significantly smaller (by $4\nu_O \sim 25$ MHz) than those presented in the original work [29]. The revised values are from later multifrequency ESEEM measurements (not shown) that, in contrast to the earlier work [29], attribute the distinct ^{17}O-hydroxo feature of the ESEEM spectrum of *hpH* SO to the high-frequency ($A/2 + \nu_O$) fundamental line rather than to the low-frequency ($A/2 - \nu_O$) fundamental line.

Fig. 5 compares the experimentally obtained *hfi* parameters of ^1H and ^{17}O (shown by horizontal shaded areas) with those calculated by DFT (shown by open circles) as a function of θ_{OH} (where θ_{OH} is a dihedral angle between the O Mo O(H) and Mo O H planes; $\theta_{OH} = 0°$ corresponds to the OH being coplanar with Mo O, $\theta_{OH} = 90°$ corresponds to OH being about parallel to Mo S(pterin), while $\theta_{OH} = 270°$ corresponds to OH being about parallel to Mo S(cysteine)). The vertical shaded areas show the ranges of θ_{OH} for *hpH* and *lpH* SO for which the experimental and calculated *hfi* constants are in agreement. Fig. 6 shows a schematic drawing of these orientations.

3. The low-pH form

Bray et al. observed that the CW EPR spectra of cSO are affected by the concentration of Cl^- in the buffer, and they therefore proposed that chloride should be located near the Mo(V) center of the *lpH* form of cSO [18]. Extended X-ray absorption fine structure (EXAFS) experiments later provided some support for this idea, but the results were inconclusive since EXAFS is not capable of distinguishing between Cl and S nuclei [30]. Nonetheless, two possibilities could be envisioned for the interaction of the proposed Cl^- with the active center of SOEs. One possibility is for the anion to directly coordinate the Mo at the open axial position of the Mo(V), trans to O_{ax}. Alternatively, the anion could associate with the positively charged substrate binding pocket and interact with the metal center through a hydrogen bonding interaction with the equatorial OH. In CW EPR spectra of model oxo-Mo(V) compounds, a directly coordinated Cl^- ligand that is *cis* to the terminal oxo group has isotropic and anisotropic *hfi* constants of ~10 MHz (for ^{35}Cl, $I = 3/2$) [31]. This result suggested that for *lpH* SO, coordination of Cl^- might also be directly detected by Cl *hfi* in the EPR spectra.

Using CW EPR, Doonan et al. revisited the question of Cl^- coordination with *lpH* SO using buffers prepared with isotopically pure $^{35}Cl^-$ and $^{37}Cl^-$ (both $I = 3/2$) [32]. They reported extremely subtle differences between the CW EPR spectra of the pure isotopic preparations, suggesting at least some influence of the Cl^- on the *lpH* form EPR spectra. From simulations of the spectrum of each isotopic preparation and the differences between the spectra, they estimated the Cl^- *hfi* to be ~3.5 MHz. The CW EPR spectra of the *lpH* SO samples obtained in the presence of Br^- and I^- showed resolved Br and I hyperfine splittings that were ~4.5 times greater than those from Cl^-. Based largely on the magnitude of the halide *hfi* values, the authors proposed that the *lpH* form of SO had direct coordination of Cl^- to the Mo(V) in an axial position *trans* to the terminal oxo group. In our pulsed EPR experiments, the ESEEM of unknown origin observed for *lpH* cSO was also tentatively attributed to the *hfi* of a chlorine nucleus [31]. It was suggested [31] that the putative chloride should be coordinated to the Mo(V) (in the axial position trans to the oxo ligand)

because it was assumed that the through-bond interaction with a more distant second-sphere Cl would result in extremely small *hfi* values.

Additional pulsed EPR experiments performed by us very clearly demonstrated that the ESEEM spectra of *lpH* SO depend on the specific chloride isotope composition of the buffer [11]. The HYSCORE spectra of *lpH* samples prepared in Cl^-, $^{35}Cl^-$, and $^{37}Cl^-$ buffers (Cl-SO, ^{35}Cl-SO, and ^{37}Cl-SO, respectively) depend on the specific Cl isotope used in the preparation, as shown in Fig. 7. As expected, the spectrum of the sample containing the natural abundance of the chloride isotopes (Cl-SO) exhibits all of the cross-peaks that are observed in the combined spectra of the samples prepared separately with ^{35}Cl and ^{37}Cl. Detailed ESEEM experiments on ^{35}Cl-SO allowed accurate estimates of both the *hfi* and *nqi* of the chloride to be made. From simulations of the spectra, the anisotropic *hfi* constant of ^{35}Cl was estimated as $|T_\perp| = 0.2 \pm 0.05$ MHz, with a_{iso} in the range of 4–5 MHz, and the *nqi* constant was estimated to be ~3 MHz. The determination of the *nqi* constant is important because this constant is sensitive to the electric field gradient created by the local electronic environment (bonds and charges) on the nucleus of interest, and it is often very useful for distinguishing between different structural possibilities (such as metal- *vs.* protein-coordinated Cl^- in this case). Qualitatively, the small ^{35}Cl *nqi* constant in the *lpH* SO spectra suggests a very symmetric electronic environment of the Cl^- ion, which contradicts the model of Cl^- coordinated to the highly positively charged Mo(V) ion.

In the absence of appropriate synthetic complexes of Mo(V) that could provide the magnetic resonance parameters for axially and equatorially coordinated Cl^- and thereby allow direct comparisons to be made with the enzyme, the detailed interpretation of the available spectroscopic parameters (*g*-values and ^{35}Cl, ^{17}O, and ^{1}H *hfi* and/or *nqi* parameters) in terms of structure was done using DFT calculations for a series of models accounting for both the inner- and outer-sphere coordination possibilities. The results of these calculations did not favor the possibility of axial coordination, in contrast to the conclusions of Doonan et al. [32]. Instead, the best overall agreement between the calculated and experimental parameters was achieved for a model that was derived directly from the X-ray crystal structure of recombinant cSO (PDB 2A99) [33], having a single Cl^- that is hydrogen-bonded to the OH ligand in the equatorial plane of the 5-coordinate Mo(V) center (Fig. 8). In this case, the calculated *nqi* constant for the ^{35}Cl atom corresponded to the experimental value, but the calculated *hfi* values were consistently underestimated compared to the experimental results. The underestimation of the *hfi* was attributed to some structural differences between the computational models and the actual Mo active site under the conditions of the EPR studies (low pH, 20 K). Steric considerations further disfavored the possibility of axial coordination, since coordination of any ligand in the position *trans* to O_{ax} would require displacement of the conserved Arg residue occupying that area (R160 in hSO). Independent support for the assignment of the Cl^- in the substrate binding pocket of the *lpH* form of SO, and not in the axial position, was later provided by EXAFS studies of the enzymes prepared in buffers containing I^-, which in contrast to Cl^- can easily be distinguished from sulfur. These EXAFS experiments showed a weak backscattering peak ~5 Å from the Mo, which was assigned to I^- [34]. This distance is equivalent to the Mo···Cl distance found in the recombinant cSO structure (pdb 2A99) [33]. Molecular dynamics simulations of the iodide and protein movements also supported the assignment of the anion to the binding pocket in the equatorial plane, as found previously from the HYSCORE data and the DFT modeling for *lpH* SO containing Cl^- [11].

For the equatorial OH ligand, the *hfi* of the ^{17}O and ^{1}H (^{2}H) nuclei were readily determined by pulsed EPR experiments [20,35]. Fig. 5 presents the experimental isotropic *hfi* constants for these nuclei together with the values estimated from DFT calculations. As is evident from Fig. 5, these *hfi* parameters restrict the OH orientations to narrow ranges around $\theta \sim$

230° and $\Theta \sim 300°$, and therefore severely constrain the possible geometry of the OH ligand. The schematic presentation in Fig. 6 clearly demonstrates the difference between the possible orientations of the equatorial OH ligand for the *lpH* and *hpH* forms of SO.

4. Oxyanion forms

4.1. The phosphate inhibited (P_i) form

The active sites of SOEs have a high binding affinity for oxyanions, and it was observed early on by CW EPR that the presence of phosphate in the buffer at low pH leads to the formation of the P_i form of SO with unique *g*-values [17]. In contrast to the usual *lpH* form, which has a very strong proton *hfi* as described above, no proton *hfi* is detected in the P_i form. These data were interpreted as indicative of the substitution of the equatorial OH ligand by phosphate. As noted above, however, no *hfi* with ^{31}P (100% $I = ½$), which would confirm such a structure, was seen in the CW EPR, although the third-derivative spectrum provided some evidence for coupling to ^{31}P [22].

In order to begin characterizing the structure of the Mo(V) center of the P_i form and to directly confirm the presence of phosphate as a ligand to Mo(V), Bray compared the EPR spectra of samples of cSO in ^{17}O-labeled phosphate buffer with those in buffer containing regular phosphate [19]. An analysis of the differences between the spectra allowed phosphate coordination to Mo(V) to be inferred, but provided little additional information about the specifics of the phosphate interaction. The ESEEM experiments, on the other hand, provided the necessary resolution to detect the ^{31}P *hfi* directly. Initially, due to the wide distribution of the *hfi* constant, it was only possible to evaluate that the ^{31}P a_{iso} could range from ~0 to ~20 MHz, which would be appropriate for the ^{31}P of phosphate located in the proposed equatorial position [23]. Later, using 2D ESEEM techniques (Fig. 9), we were able to observe the ^{31}P fundamental lines directly and confirm the initial estimate of the *hfi*. The direct detection of the ^{31}P unequivocally confirmed the proposed PO_4^{3-} coordination to the Mo center in the P_i form of SO [24].

4.2. The “blocked” form

Unlike vertebrate SO, plant SO contains no integral heme centers, and the type of EPR signal it produces depends on the method of reduction of the enzyme. Reduction of the fully oxidized plant enzyme using sulfite at low pH (followed by one-electron oxidation by ferricyanide to obtain the Mo(V) state), for example, produces an EPR signal that is different from the one obtained by one-electron reduction from Mo(VI) using titanium(III) citrate [12]. In the latter case, the regular *lpH* form is obtained that exhibits a strong proton coupling, indicative of an OH ligand. In the case of sulfite reduction, however, no proton splittings are observed, although the principal *g*-values are similar to those of the *lpH* form.

One explanation for the absence of a proton-containing ligand is that sulfate (product) is coordinated to the Mo(V) center in the place of OH, producing a “blocked” enzyme-product complex (**4** in Scheme 1) [12]. Alternatively, the signal could also arise from the complex with equatorially coordinated sulfite (**5** in Scheme 1), because the substrate (sulfite) is typically present in ~20-fold excess during the reduction. The formation of a sulfite form was previously proposed from the different EPR spectrum observed for cSO reduced by sulfite in Mes (4-morpholine-ethanesulphonic acid) buffer at pH 6.5–6.6 [16]. In contrast to the P_i form, however, the direct detection of a sulfite or sulfate ligand either by CW EPR or by pulsed methods is far more difficult. Sulfite exchanges its oxygen atoms with water very rapidly [36], therefore ^{17}O labeling experiments would not be informative. Moreover, ^{32}S (95%, $I = 0$) is magnetically silent. Direct spectroscopic evidence for a sulfur-containing ligand was initially obtained from pulsed EPR spectra of plant SO that had been reduced

with ^{33}S-labeled sulfite [13]. Subsequently it was shown (*vide infra*) that the pulsed EPR spectra of all forms of hSO [37], as well as SDH [38], exhibit coupling to ^{33}S when reduced with labeled sulfite at low pH in the absence of chloride.

Conclusive assignment of the sulfur-containing ligand as either sulfite or sulfate required isotopic labeling with ^{33}S (I = 3/2) and ^{17}O (I = 5/2), variable frequency pulsed EPR spectroscopy, and a full comparative analysis of the ^{17}O and ^{33}S magnetic resonance parameters with those calculated for a series of DFT models for the sulfite and sulfate possibilities [24]. ESEEM studies of plant SO from *Arabidopsis thaliana* that had been reduced with sulfite labeled with ^{33}S conclusively demonstrated the presence of a coordinated sulfur-containing ligand [13]. The ^{33}S isotropic *hfi* constant determined in these experiments was small (a_{iso} ~ 3 MHz), while the quadrupole coupling constant was large (e^2Qq/h ~ 40 MHz). Reduction of the R160Q mutant of hSO with ^{33}S-labeled sulfite also showed the presence of a sulfur-containing ligand, with a_{iso} = 2.1 MHz and e^2Qq/h = 36 MHz (Fig. 10) [25]. Subsequent investigations of *wt* hSO and several hSO mutants that had been reduced at low pH with ^{33}S-labeled sulfite showed that a similar Mo(V) species with a sulfur-containing ligand was formed in all cases when the reduction was carried out in the strict absence of chloride [37]. Reduction of SDH under these conditions also resulted in a sulfur-containing ligand with similar values for a_{iso} and the quadrupole coupling constant [38].

Initially, the ^{33}S parameters were interpreted as arising from bound sulfate (product), **4** in Scheme 1. However, the observed quadrupole coupling constants (36–40 MHz) seemed unusually large for sulfur in a tetrahedral environment. Unfortunately, no model coordination compounds are available to provide benchmark hyperfine and quadrupole parameters for ^{33}S in sulfate or sulfite ligands. Therefore, DFT calculations were used to determine the nature of the sulfur-containing ligand. Preliminary calculations on a truncated model suggested that sulfite better fits the pulsed EPR data than sulfate [39]. Sulfite ligation was verified by calculations on a much larger model (>250 atoms), shown in Table 1 and Fig. 11 [24].

The pulsed EPR spectra of the R160Q mutant of hSO in $H_2{}^{17}O$ have also been used to determine the structure of its Mo(V) center. Couplings to two types of ^{17}O atoms were observed, and initially these were assigned to a coordinated ^{17}O of the sulfur-containing ligand in the equatorial position and to the axial oxo ligand [25]. However, the quadrupole coupling constant for the presumed axial oxo group was substantially larger than the *nqi* constants in five-coordinate model oxo compounds [40] and in the *hpH* form of SO [41] (e^2Qq/h ~ 5 MHz in R160Q SO *vs.* 1.5 MHz in *hpH* SO). This difference was tentatively explained as due to weak axial coordination of Gln 160 *trans* to the oxo ligand. This hypothesis was indirectly supported by an ESEEM study of a six-coordinate oxo-Mo(V) complex, for which a relatively large oxo-^{17}O *nqi* constant (e^2Qq/h ~ 3 MHz) was found [25]. Later studies have revealed, however, that the oxo ligand does not readily exchange at low pH, while sulfite rapidly exchanges its oxygen atoms in H_2O [36]. Therefore, it was suggested that the two ^{17}O signals arise from the coordinated and remote ^{17}O atoms of the sulfur-containing ligand. This hypothesis was verified by showing that ^{17}O peaks disappear upon addition of phosphate (Fig. 12), which displaces the sulfur-containing ligand (the oxygen atoms of phosphate do not exchange in $H_2{}^{17}O$), and by the appearance of 31P features in the HYSCORE spectrum [24]. Interestingly, the ^{31}P *hfi* constant in the *P*i form of R160Q hSO (21–43 MHz [24]) is significantly larger than that of *wt* hSO (4–11 MHz, see Fig. 9). This is attributed to differences in the orientation of the phosphate ligand with respect to the Mo(V) d_{xy} orbital in the two species, resulting in increased spin population on the phosphorus of the mutant enzyme compared to that of the *wt* enzyme. The experimental ^{17}O parameters for R160Q hSO and the parameters calculated from DFT for

sulfate and sulfite coordination are given in Table 1. The combined experimental and DFT results for R160Q hSO clearly demonstrate that reduction of SO with excess sulfite at low pH produces species **5** of Scheme 1, with bound sulfite as a ligand.

4.3. Other oxyanion forms

Addition of arsenate to sulfite-reduced hSO produced a complex CW EPR spectrum due to coupling with ^{75}As (100% $I = 3/2$). The EPR evidence for coordinated arsenate was supported by the observation of a Mo···As peak of 3.20 Å in the Mo K-edge EXAFS [26]. This result is consistent with monodentate coordination of arsenate through an oxygen atom, as occurs for phosphate in the P_i form of SO, and suggests that this is also the mode of interaction of the product (sulfate) with the reduced Mo center (**2** in Scheme 1).

5. Conclusions

The first CW EPR spectra for cSO were reported in 1971 [42], and the sensitivity of the spectra to pH and anions in the media led to early identification of the *lpH*, *hpH*, and P_i forms of vertebrate SOs [17]. The X-ray crystal structure of cSO [6] provided a framework for interpreting the EPR results as arising from a five-coordinate pseudo-square-pyramidal Mo with an axial oxo ligand, three equatorial sulfur donor atoms, and an exchangeable solvent-exposed equatorial ligand that varies during the catalytic cycle. However, determination of the structures of the various Mo(V) forms of SOEs has required combining variable-frequency pulsed EPR methods [43,44], isotopic labeling [13,25,41], synthesis of model compounds [25,40], and DFT calculations [11,24]. These combined integrated studies have revealed several specific features about SOEs:

1. The axial oxo ligand is exchangeable at high pH. The ^{17}O *hfi* and *nqi* parameters of this ligand vary little among the various Mo(V) forms of SOEs.
2. The *lpH* form of vertebrate SOs has a chloride ion that is located in the 2nd coordination sphere, hydrogen-bonded to the equatorial OH ligand, and in a nearly spherical environment of water molecules and other hydrogen bond donors from side chains of the protein.
3. The *hpH* form of SOEs has a coordinated OH ligand that adopts an orientation with the OH bond nearly parallel with the Mo O bond; this leads to a very weak isotropic *hfi* of the OH proton, but the anisotropic *hfi* is relatively strong.
4. The P_i form has a monodentate phosphate ligand.
5. The “blocked” form is commonly formed for hSOs at low pH in the absence of chloride and contains a monodentate sulfite ligand.

Acknowledgments

We gratefully acknowledge support of this research by the National Institutes of Health (GM-037773 to JHE). We thank the NSF (DBI-0139459, DBI-9604939, BIR-9224431) and the NIH (S10RR020959, 1S10RR26416-01) for funds for the development of the pulsed EPR Facility at the University of Arizona. A portion of the research was performed using EMSL, a national scientific user facility sponsored by the Department of Energy’s Office of Biological and Environmental Research and located at Pacific Northwest National Laboratory.

Abbreviations

SO	sulfite oxidase
SDH	sulfite dehydrogenase

SOE	sulfite oxidizing enzyme
EPR	electron paramagnetic resonance
ESEEM	electron spin echo envelope modulation
IET	intramolecular electron transfer
DFT	density functional theory
hpH	high pH
lpH	low pH
P_i	phosphate inhibited
hfi	hyperfine interaction
nqi	nuclear quadrupole interaction
HYSCORE	hyperfine sublevel correlation
Moco	molybdenum cofactor

References

1. Hille R. Chem Rev. 1996; 96:2757. [PubMed: 11848841]
2. Kappler, U. Microbial Sulfur Metabolism. Friedrich, CG.; Dahl, C., editors. Springer; Berlin: 2008. p. 151-169.
3. Feng C, Tollin G, Enemark JH. Biochim Biophys Acta. 2007; 1774:527. [PubMed: 17459792]
4. Hänsch R, Lang C, Riebeseel E, Lindigkeit R, Gessler A, Rennenberg H, Mendel RR. J Biol Chem. 2006; 281:6884. [PubMed: 16407262]
5. Kappler U, Friedrich CG, Truper HG, Dahl C. Arch Microbiol. 2001; 175:102. [PubMed: 11285738]
6. Kisker C, Schindelin H, Pacheco A, Wehbi WA, Garrett RM, Rajagopalan KV, Enemark JH, Rees DC. Cell. 1997; 91:973. [PubMed: 9428520]
7. Schrader N, Fischer K, Theis K, Mendel RR, Schwarz G, Kisker C. Structure. 2003; 11:1251. [PubMed: 14527393]
8. Kappler U, Bailey S. J Biol Chem. 2005; 280:24999. [PubMed: 15863498]
9. George GN, Pickering IJ, Kisker C. Inorg Chem. 1999; 38:2539.
10. Doonan CJ, Wilson HL, Rajagopalan KV, Garrett RM, Bennett B, Prince RC, George GN. J Am Chem Soc. 2007; 129:9421. [PubMed: 17608478]
11. Klein EL, Astashkin AV, Ganyushin D, Riplinger C, Johnson-Winters K, Neese F, Enemark JH. Inorg Chem. 2009; 48:4743. [PubMed: 19402624]
12. Astashkin AV, Hood BL, Feng CJ, Hille R, Mendel RR, Raitsimring AM, Enemark JH. Biochemistry. 2005; 44:13274. [PubMed: 16201753]
13. Astashkin AV, Johnson-Winters K, Klein EL, Byrne RS, Hille R, Raitsimring AM, Enemark JH. J Am Chem Soc. 2007; 129:14800. [PubMed: 17983221]
14. Bailey S, Rapson T, Johnson-Winters K, Astashkin AV, Enemark JH, Kappler U. J Biol Chem. 2009; 284:2053. [PubMed: 19004819]
15. Emesh S, Rapson TD, Rajapakshe A, Kappler U, Bernhardt PV, Tollin G, Enemark JH. Biochemistry. 2009; 48:2156. [PubMed: 19226119]
16. Bray RC, Lamy MT, Gutteridge S, Wilkinson T. Biochem J. 1982; 201:241. [PubMed: 6282260]
17. Lamy MT, Gutteridge S, Bray RC. Biochem J. 1980; 185:397. [PubMed: 6249254]
18. Bray RC, Gutteridge S, Lamy MT, Wilkinson T. Biochem J. 1983; 211:227. [PubMed: 6307274]
19. Gutteridge S, Lamy MT, Bray RC. Biochem J. 1980; 191:285. [PubMed: 6258584]
20. Raitsimring AM, Pacheco A, Enemark JH. J Am Chem Soc. 1998; 120:11263.

21. Astashkin AV, Mader ML, Pacheco A, Enemark JH, Raitsimring AM. J Am Chem Soc. 2000; 122:5294.
22. George GN, Prince RC, Kipke CA, Sunde RA, Enemark JH. Biochem J. 1988; 256:307. [PubMed: 2851985]
23. Pacheco A, Basu P, Borbat P, Raitsimring AM, Enemark JH. Inorg Chem. 1996; 35:7001. [PubMed: 11666879]
24. Klein EL, Raitsimring AM, Astashkin AV, Rajapakshe A, Johnson-Winters K, Arnold AR, Potapov A, Goldfarb D, Enemark JH. Inorg Chem. 2012; 51:1408. [PubMed: 22225516]
25. Astashkin AV, Johnson-Winters K, Klein EL, Feng CJ, Wilson HL, Rajagopalan KV, Raitsimring AK, Enemark JH. J Am Chem Soc. 2008; 130:8471. [PubMed: 18529001]
26. George GN, Garrett RM, Graf T, Prince RC, Rajagopalan KV. J Am Chem Soc. 1998; 120:4522.
27. George GN. J Magn Reson. 1985; 64:384.
28. Cramer SP, Johnson JL, Rajagopalan KV, Sorrell TN. Biochem Biophys Res Commun. 1979; 91:434. [PubMed: 229850]
29. Astashkin AV, Klein EL, Ganyushin D, Johnson-Winters K, Neese F, Kappler U, Enemark JH. Phys Chem Chem Phys. 2009; 11:6733. [PubMed: 19639147]
30. George GN, Kipke CA, Prince RC, Sunde RA, Enemark JH, Cramer SP. Biochemistry. 1989; 28:5075. [PubMed: 2548601]
31. Astashkin AV, Klein EL, Enemark JH. Inorg J Biochem. 2007; 101:1623.
32. Doonan CJ, Wilson HL, Bennett B, Prince RC, Rajagopalan KV, George GN. Inorg Chem. 2008; 47:2033. [PubMed: 18271529]
33. Karakas E, Wilson HL, Graf TN, Xiang S, Jaramillo-Busquets S, Rajagopalan KV, Kisker C. J Biol Chem. 2005; 280:33506. [PubMed: 16048997]
34. Pushie MJ, Doonan CJ, Wison HL, Rajagopalan KV, George GN. Inorg Chem. 2011; 50:9406. [PubMed: 21894921]
35. Astashkin AV, Enemark JH, Raitsimring AM. Concepts Magn Reson B (Magn Reson Eng). 2006; 29B:125.
36. Betts RH, Voss RH. Can J Chem. 1970; 48:2035.
37. Rajapakshe A, Johnson-Winters K, Nordstrom AR, Meyers KT, Emesh S, Astashkin AV, Enemark JH. Biochemistry. 2010; 49:5154. [PubMed: 20491442]
38. Rapson TD, Astashkin AV, Johnson-Winters K, Bernhardt PV, Kappler U, Raitsimring AM, Enemark JH. J Biol Inorg Chem. 2010; 15:505. [PubMed: 20084533]
39. Enemark JH, Raitsimring AM, Astashkin AV, Klein EL. Faraday Discuss. 2011; 148:249. [PubMed: 21322488]
40. Astashkin AV, Neese F, Raitsimring AM, Cooney JJA, Bultman E, Enemark JH. J Am Chem Soc. 2005; 127:16713. [PubMed: 16305262]
41. Astashkin AV, Feng C, Raitsimring AM, Enemark JH. J Am Chem Soc. 2005; 127:502. [PubMed: 15643856]
42. Cohen HJFI, Rajagopalan KV. J Biol Chem. 1971; 246:374. [PubMed: 5100417]
43. Enemark JH, Astashkin AV, Raitsimring AM. Dalton Trans. 2006:3501. [PubMed: 16855750]
44. Enemark, JH.; Astashkin, AV.; Raitsimring, AM. High-resolution EPR spectroscopy of Mo enzymes. Sulfite oxidases: structural and functional implications. In: Hanson, G.; Berliner, LJ., editors. Biological Magnetic Resonance. Vol. 29. Springer; New York: 2010. p. 122-162.

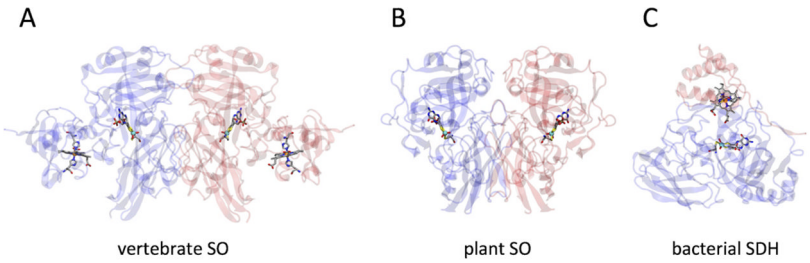

Fig. 1.

Representative wild-type protein structures of vertebrate SO, plant SO, and bacterial SDH. (A) Vertebrate SO (1.7 Å chicken liver SO; pdb ID = 1SOX) is a 110 kDa α_2 -dimeric protein located in the mitochondrial intermembrane space. Each subunit consists of a *b*-type-heme domain and a Moco domain, which are connected to each other by a flexible tether that is disordered in the crystal structure. (B) Plant SO (2.6 Å *A. thaliana* SO; pdb ID = 1OGP) is a 90 kDa α_2 -dimeric protein located in the peroxisome. In contrast to all other SOEs, plant SO contains no heme centers since molecular oxygen serves directly as the terminal electron acceptor in plants. (C) Bacterial SDH (1.8 Å *S. novella* SDH; pdb ID = 2BLF) is a 50 kDa αβ-dimeric protein located in the periplasm that consists of a Moco subunit and *c*-type-heme subunit. The metal cofactors and metal-coordinated amino acids in each structure are displayed as ball-and-stick figures for clarity.

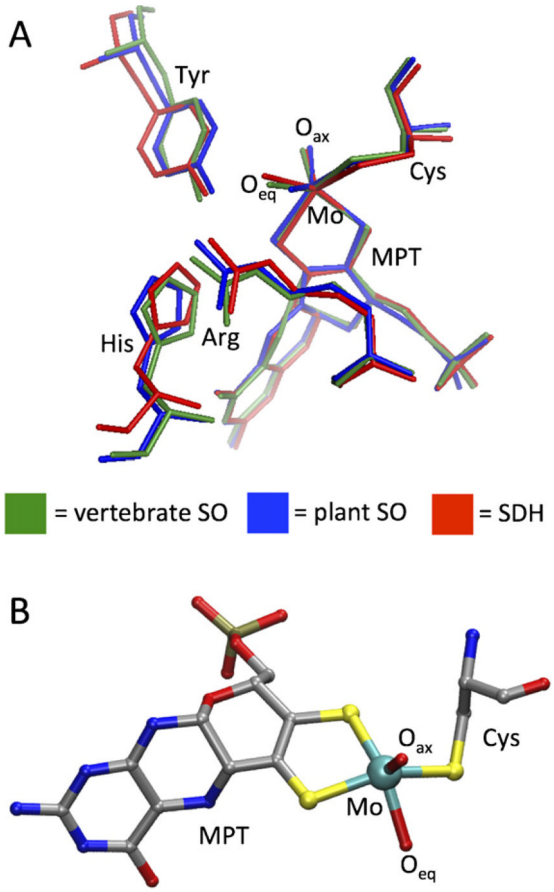

Fig. 2.

The active site structure of SOEs. (A) Overlay view of the SO and SDH active sites, including selected nearby conserved residues. (B) Ball-and-stick representation of the fully oxidized Moco center, shown with the conserved Cys residue coordinated to Mo.

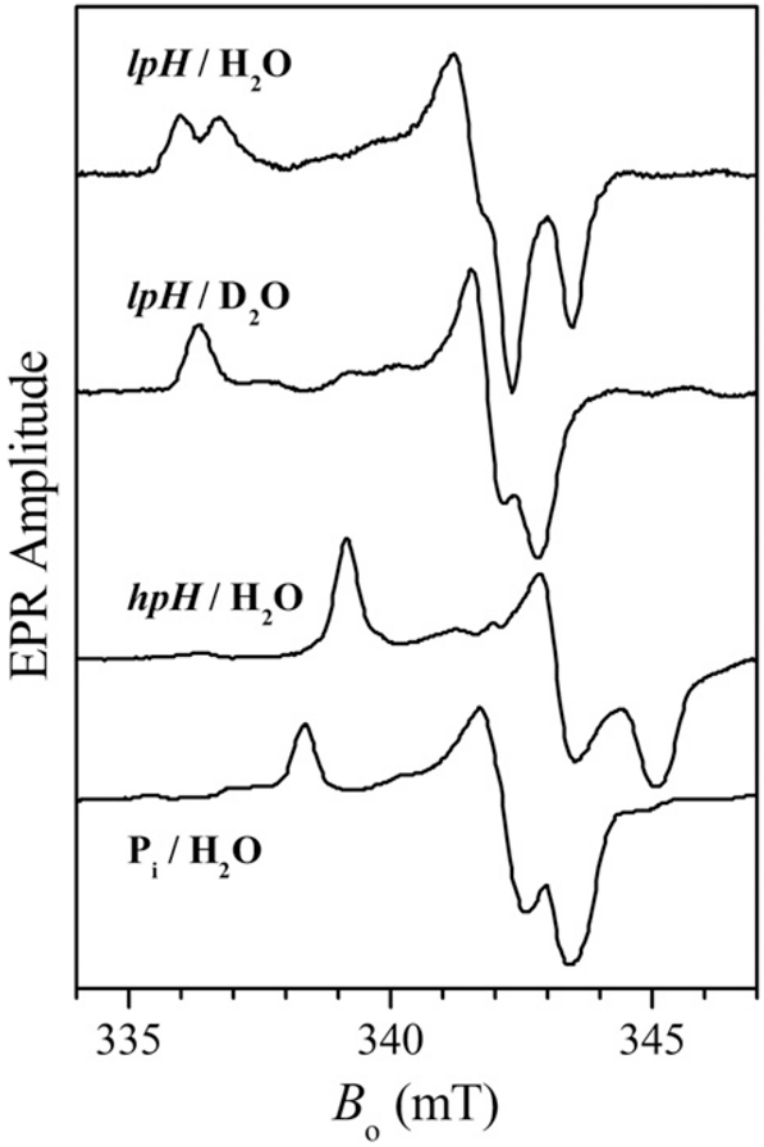

Fig. 3.
X-band CW EPR spectra of the *lpH*, *hpH*, and P_i forms of SO. Note that the *lpH* form shows resolved splittings from an exchangeable proton, which collapse in D_2 O solution.

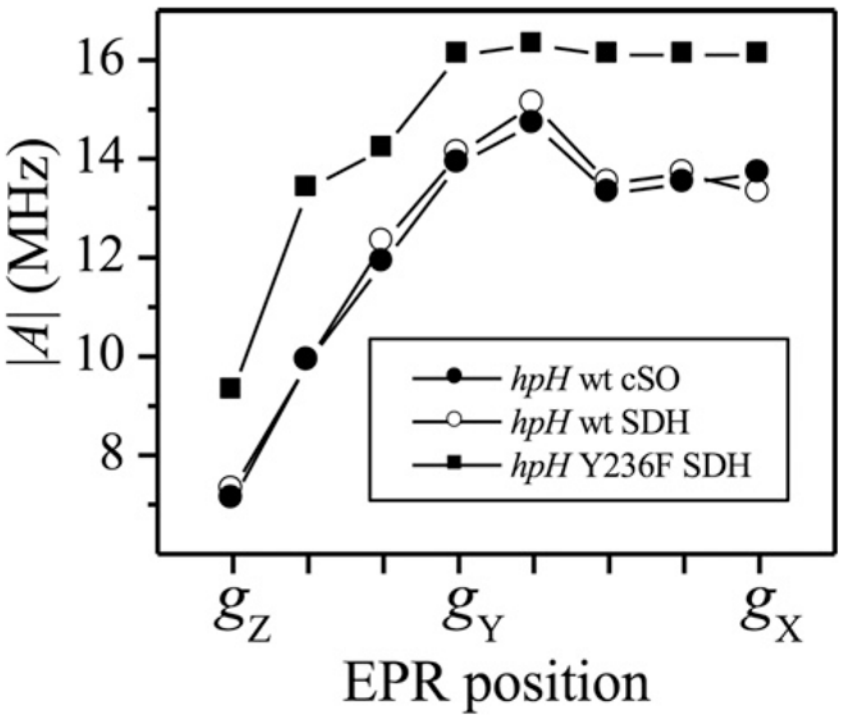

Fig. 4.

Total hyperfine constants (including the isotropic and anisotropic contributions) of the equatorial ^{17}O ligand for several different *hpH* SOEs as a function of the EPR position, calculated from the position of the experimental fundamental line ν_β as $|A| = 2|(\nu_\beta - \nu_O)|$.

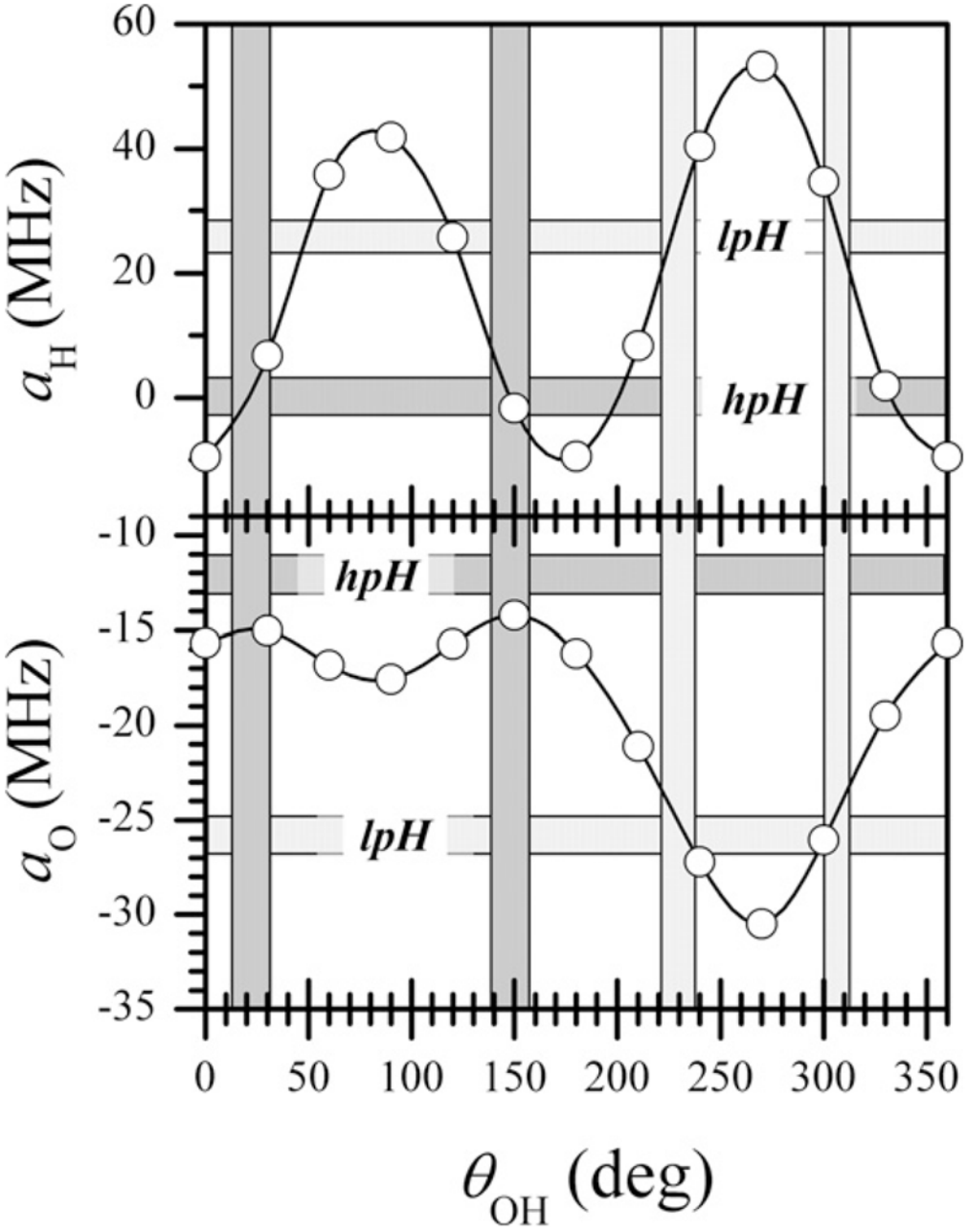

Fig. 5.

Open circles, ^{1}H and ^{17}O isotropic *hfi* constants calculated by DFT as a function of θ_{OH}, where θ_{OH} is a dihedral angle between the O Mo O(H) and Mo O H planes; $\theta_{OH} = 0°$ corresponds to Mo O H being exactly coplanar with O Mo O(H) and the OH proton being oriented toward O_{ax}, $\theta_{OH} = ~90°$ corresponds to the OH proton being oriented away from S(cysteine), while $\theta_{OH} = ~270°$ corresponds to the OH proton being oriented toward S(cysteine). Horizontal dark shaded areas indicate the experimental *hfi* values for *hpH* SO; horizontal light shaded areas indicate the experimental *hfi* values for *lpH* SO. The vertical dark shaded areas show the ranges of θ_{OH} for which the experimental and calculated *hfi* constants are in agreement for *hpH*, and the vertical light shaded areas show the corresponding ranges of θ_{OH} for *lpH* SO.

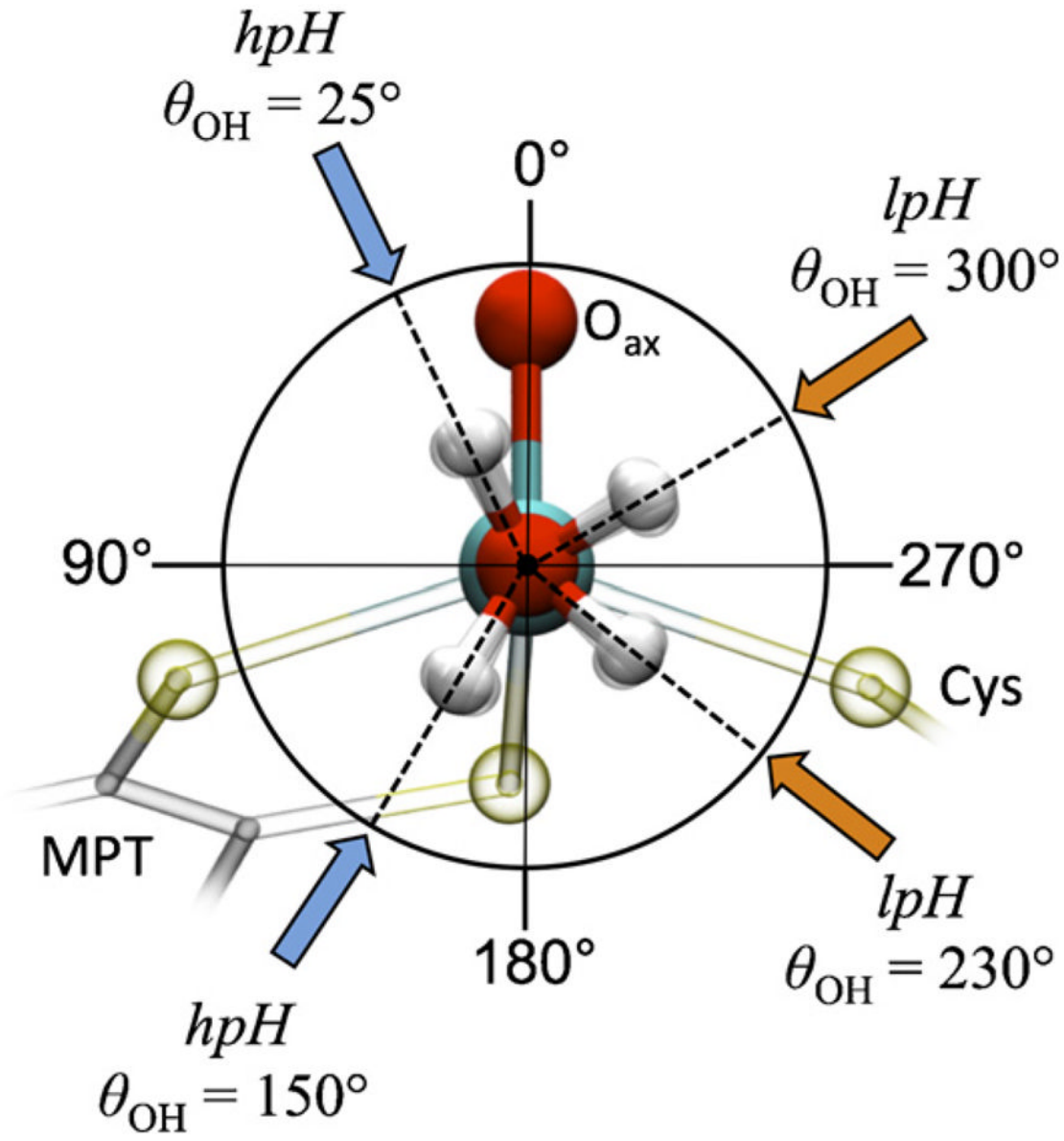

Fig. 6.

Projection along the equatorial Mo O(H) bond of SO, showing the possible orientations of the OH ligand in the *hpH* (blue arrows) and *lpH* (orange arrows) forms, as determined by the general agreement of the experimentally measured and DFT-calculated *hfi* values shown in Fig. 5. θ_{OH} is defined in Fig. 5 caption.

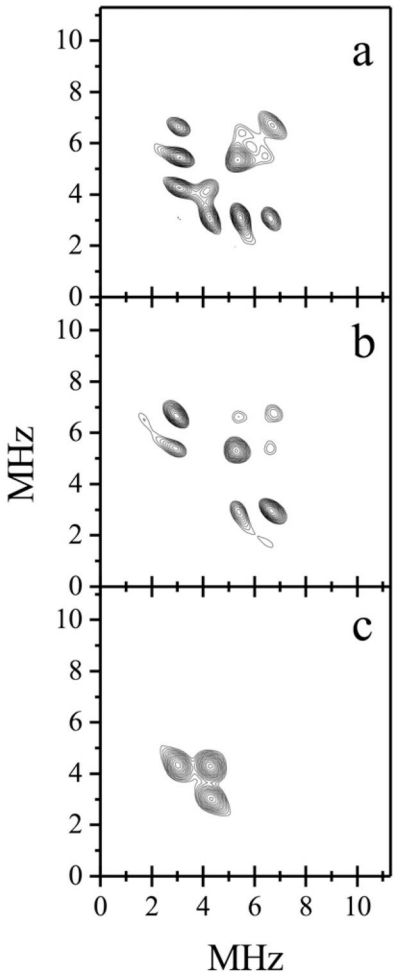

Fig. 7.

Panels a, b, and c, (++) quadrants of HYSCORE spectra of *lpH* Cl-SO, ^{35}Cl-SO and ^{37}Cl-SO, respectively. Experimental conditions: ν_{mw} = 29.562 GHz; B_o = 1075.6 mT (g_y); time interval between the first and second mw pulses, τ = 200 ns; mw pulses, 15, 15, 27, 15 ns; temperature, 21 K.

Source: Reprinted with permission from Ref. [11]. Copyright 2009 American Chemical Society.

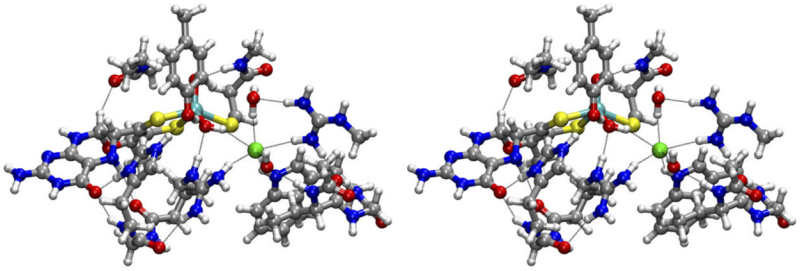

Fig. 8.

Stereo view (cross-eye) of the geometry-optimized computational model that was obtained from geometry optimization of the X-ray crystal coordinates from recombinant cSO with Cl^- near the Mo center (PDB 2A99).

Source: Reprinted with permission from Ref. [11]. Copyright 2009 American Chemical Society.

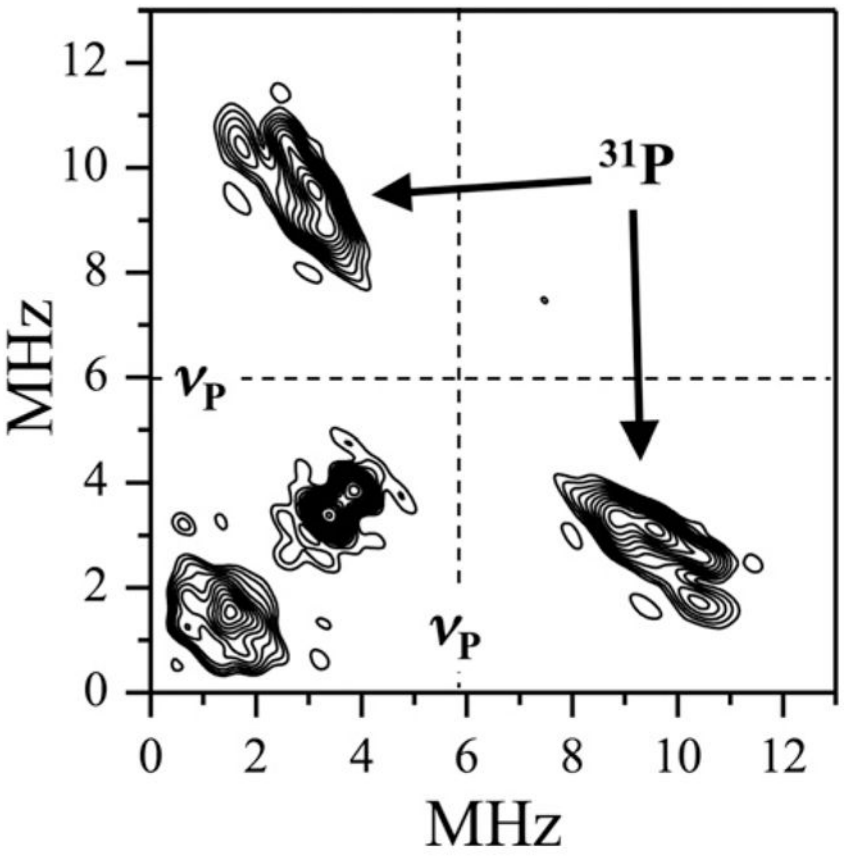

Fig. 9.

HYSCORE spectrum of the hSO P_i form collected at the g_y position. Experimental conditions: mw frequency = 9.51 MHz; B_o = 344.8 mT; time interval between the 1st and 2nd pulses = 180 ns; mw pulses, 11, 11, 13, 11 ns; temperature, 21 K. The ^{31}P Zeeman frequency, ν_p, is indicated by dashed lines. The 31 P cross peaks are marked by arrows, and the magnitude of *hfi*, evaluated from their position, spreads between 4 and 11 MHz.

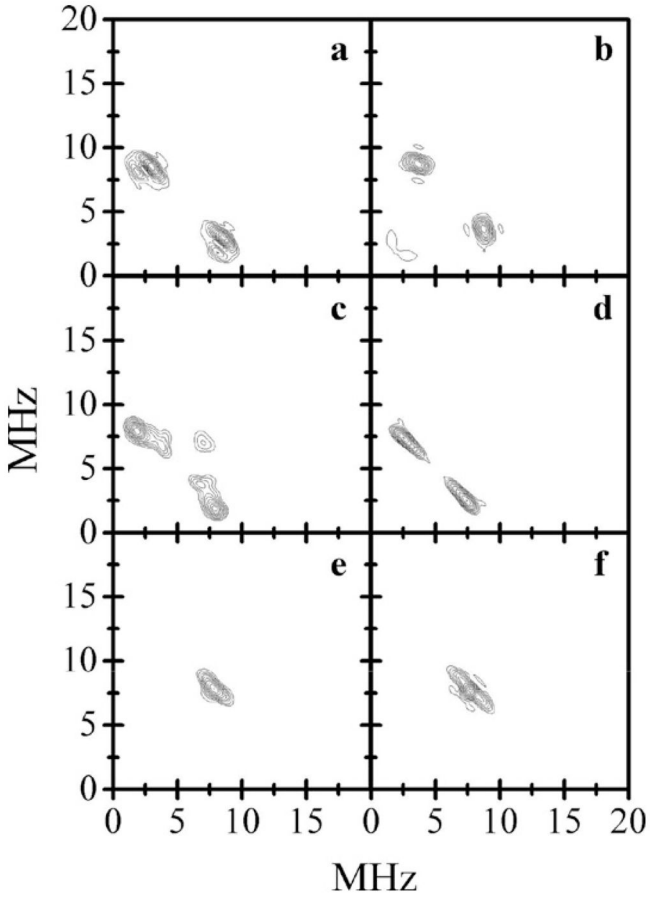

Fig. 10.

Panels a, c, and e, the (++) quadrants of the HYSCORE spectra of ^{33}S-R160Q SO (Species 1) obtained at the g_z, g_y, and g_x EPR turning points, respectively (B_o = 1060.8, 1078.8, and 1088.6 mT, respectively). The spectra shown represent sums of the spectra obtained at time intervals between the first and second mw pulses τ = 170 and 200 ns. Other experimental conditions: ν_{mw} = 29.650 GHz; mw pulses, 11, 11, 21, and 11 ns; temperature, 20 K. Panels b, d, and f, simulated HYSCORE spectra for g_z, g_y, and g_x at the EPR turning points, respectively. Simulation parameters: a_{iso} = 2.1 MHz, anisotropic *hfi* tensor in the principal axes system, (T_{11}, T_{22}, T_{33}) = (−4.1, 2.5, 1.6) MHz; e^2Qq/h = 36 MHz; η = 0.2; Euler angles for the orientation of the *hfi* tensor in the *g*-frame: ϕ_h = 20°, θ_h = 10°, Ψ_h = 20°; Euler angles for the orientation of the *nqi* tensor with respect to the g-frame: ϕ_q = 90°, θ_q = 90°, Ψ_q = 0°. The simulated spectra (as with the experimental ones) represent sums of the spectra calculated for τ = 170 and 200 ns.

Source: Reprinted with permission from Ref. [25]. Copyright 2008 American Chemical Society.

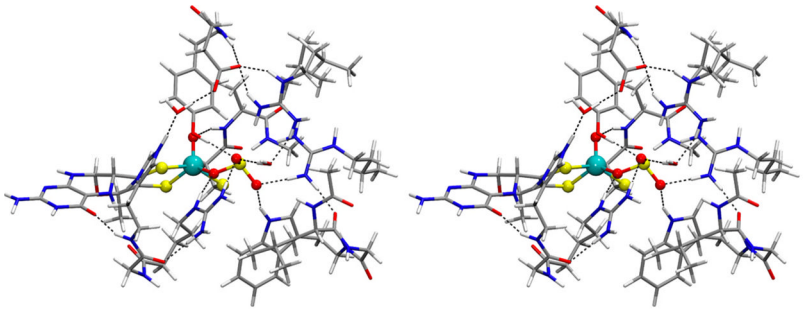

Fig. 11.
Stereo view (cross-eye) representation of the energy-minimized sulfite-bound SO model. The magnetic resonance parameters calculated for this model are provided in Table 1. *Source*: Reprinted with permission from Ref. [24]. Copyright 2012 American Chemical Society.

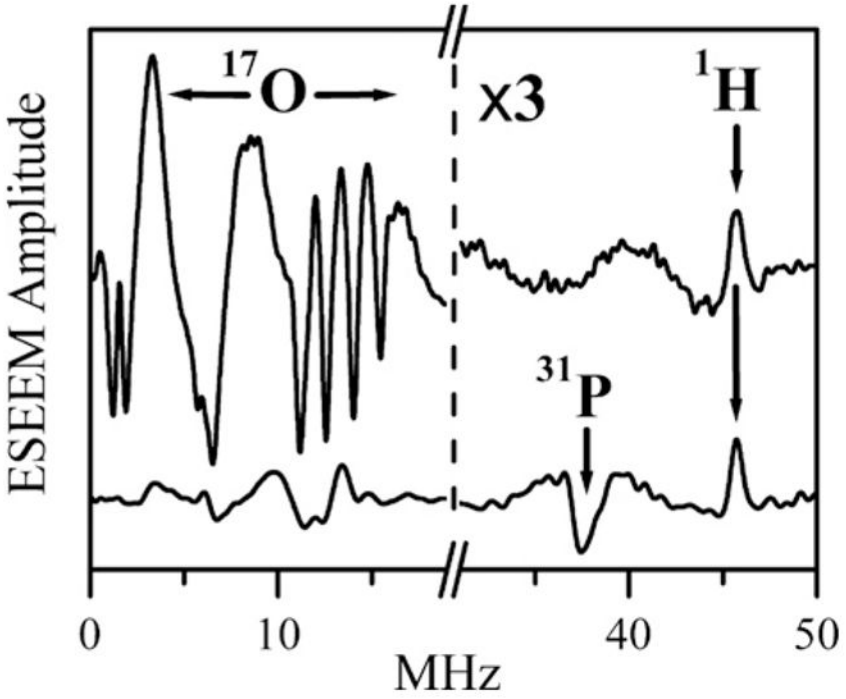

Fig. 12.

K_a -band two-pulse ESEEM spectra (cosine FT) of Species 1 (upper trace) and Species 1P (lower trace). Species 1P was prepared as described in reference 24 by adding a solution of phosphate (prepared with ^{17}O-enriched water) to a solution of Species 1 (also in ^{17}O-enriched water) at pH ~ 5.4 until the final concentration of phosphate in the solution was 700 mM. Experimental conditions: mw frequency = 30.068 GHz; B_o = 1074 mT; mw pulses, 2 × 12 ns; temperature, 21 K. For clarity, the modulation amplitudes to the right of the break in the *x*-axis have been magnified by a factor of 3. The proton matrix line is marked by the arrow labeled "^{1}H" (at ~46 MHz, which corresponds to the ^{1}H Larmor frequency, ν_H). Likewise, the arrow labeled "^{31}P" indicates the position of the sum combination line of ^{31}P (ν_σ = ~37.5 MHz), which is close to double the Larmor frequency of 31 P at this magnetic field, $2\nu_p \approx 37.1$ MHz.

Source: Reprinted with permission from Ref. [24]. Copyright 2012 American Chemical Society.

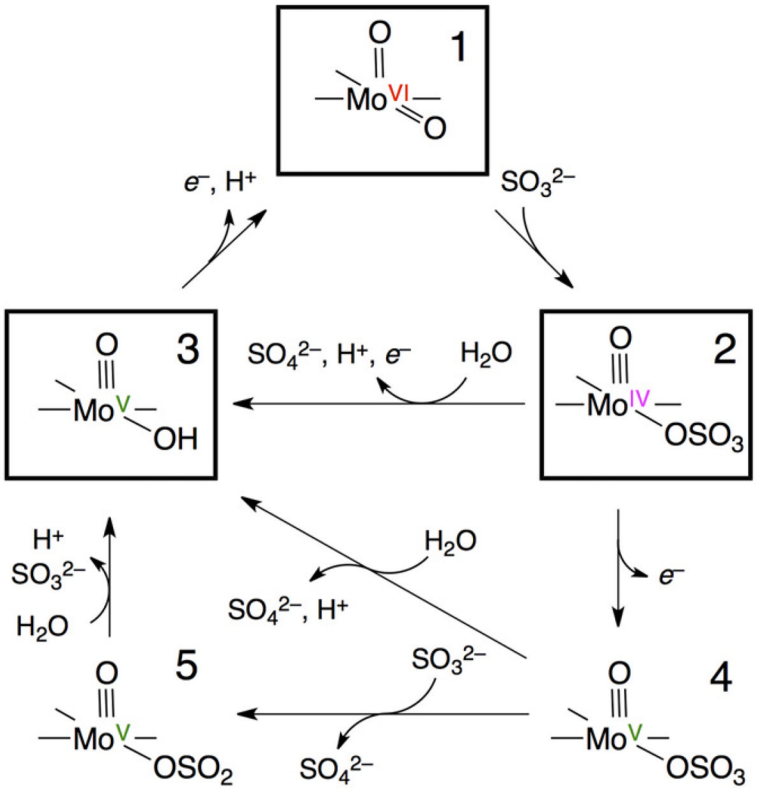

Scheme 1.

The proposed catalytic cycle of SOEs. Boxes surround the principal chemical intermediates (**1**–**3**). The formation of the sulfite (**5**) and/or sulfate (**4**) Mo(V) species from the Mo(IV) enzyme-product complex (**3**) at low pH could be achieved as shown in the lower part of the scheme.

Table 1

Experimental magnetic resonance parameters for *wt* and mutant "blocked" forms of SO and DFT-calculated magnetic resonance parameters for sulfate- and sulfite-bound SO models.[a]

Species		*hfi*		*nqi*		Ref.
		a_{iso} (MHz)	(T_{11}, T_{22}, T_{33}) (MHz)	e^2Qq/h (MHz)	h	
Blocked R160Q hSO	^{33}S	2.1	(1.6, 2.5, −4.1)	36	0.2	[24]
	$^{17}O_{coordinated}$	−9	(5, 5, −10)	7	–	
	$^{17}O_{remote}$	−4.5	(1.25, 1.25, −2.5)	5	–	
Blocked wt hSO[b,c]	^{33}S	2.6	(−0.3, −0.3, 0.6)	36	–	[37]
Blocked At-SO [b]	^{33}S	3.3	(1.3, 1.5, −2.8)	40	0	[13]
SO-sulfate (DFT)	^{33}S	3.33	(−0.53, −0.40, 0.92)	4.4	0.7	[24]
	$^{17}O_{coordinated}$	−9.56	(6.06, 5.17, −11.22)	10.9	0.3	
	$^{17}O_{remote}$	−1.23 (a)	(1.18, 1.17, −2.35)	10.6	0.1	
		0.02 (b)	(0.00, −0.36, 0.36)	10.5	0.1	
		0.01 (c)	(0.00, −0.27, 0.27)	10.9	0.1	
	$^{17}O_{oxo}$	3.26	(−3.71, −2.34, 6.04)	1.2	1.0	
SO-sulfite (DFT)	^{33}S	1.91	(−0.69, −0.45, 1.14)	27.9	0.2	[24]
	$^{17}O_{coordinated}$	−11.09	(9.34, 8.41, −17.75)	9.6	0.4	
	$^{17}O_{remote}$	−1.71 (a)	(1.66, 1.60, −3.26)	9.5	0.3	
		−0.10 (b)	(0.08, 0.45, −0.53)	9.9	0.1	
	$^{17}O_{oxo}$	3.61	(−4.38, −0.24, 4.62)	1.1	1.0	

[a] Reprinted with permission from Ref. [24]. Copyright 2012 American Chemical Society.

[b] The ^{17}O magnetic resonance parameters for these species have not been fully evaluated.

[c] The *blocked* form of this enzyme was obtained only under low-pH conditions in the strict absence of Cl^-.